NUCLEAR INSTRUMENTS AND METHODS 138 (1976) 93–104; © NORTH-HOLLAND PUBLISHING CO.

RESPONSE OF PLASTIC SCINTILLATOR DETECTORS TO HEAVY IONS, $Z \leq 35$, $E \leq 170$ MeV*

F. D. BECCHETTI†

Physics Department, The University of Michigan, Ann Arbor, Michigan 48109, U.S.A.

C. E. THORN and M. J. LEVINE

Physics Department, Brookhaven National Laboratory, Upton, New York 11973, U.S.A.

Received 2 July 1976

The fluorescent response, L, of plastic scintillators such as NE102 has been measured for a variety of heavy ions, $Z = 1$–35, at near-normal incidence with energies ranging from a few MeV to over a hundred MeV. The response in general is non-linear with $L \propto f(Z, A)E^{1.6}$ in the region $E/A < 15$ MeV/amu. The light output is best described however, as a function of the ion range in the scintillator, R, with $L \propto Z^{1.22}(R - 0.04Z)$, where R is in mg/cm^2. Such an expression also appears to describe the response of other scintillators, such as NaI(Tl), for heavy ions. Scintillation efficiency, dL/dE, and specific fluorescence, dL/dx, have been deduced from the plastic scintillator data. These quantities do not appear to be simple functions of the ion energy loss, dE/dx. The results can be described using simple models which include the effects of secondary electrons, however.

1. Introduction

Organic, plastic scintillators are widely employed in focal-plane counters for nuclear-particle magnetic spectrometers[1]) as they can provide simultaneously fast timing and energy-loss information. A serious problem, however, has been the lack of quantitative information on the response of plastic scintillators to energetic heavy ions. While some data are available on the response of heavy ions in CsI [2]), NaI [3]), and in thin film plastic detectors[4,5]) (TFD), these data cannot be easily extrapolated to predict with sufficient accuracy the response of ions stopped in plastic scintillators, such as NE102 [6]). Also, other features such as the resolution of the scintillator response is of interest and, again, these cannot be deduced directly from other data.

Besides pragmatic considerations, scintillator response data for heavy ions provide a good test of scintillation theories[7–10]). These theories have widespread applications in describing many related phenomena: biological and material radiation damage, dosimeter response, liquid and solid scintillator response, and track profiles in photographic plates and plastic track detectors[9]). The latter are important in the identification of cosmic-ray events in photographic emulsion and plastic track detectors[11]).

In this paper we present data for the luminescent response of commercially-produced organic plastic scintillators to a variety of energetic heavy ions, $Z = 1$–35, $E \leq 170$ MeV, at near-normal incidence. Preliminary results have been reported elsewhere[12]).

TABLE 1

Accelerated beams.

	Ion	Beam energy (MeV)
U. Michigan (cyclotron)	$^{2}H^{1+}$	35
	$^{3}He^{1,2+}$	26, 46
	$^{4}He^{1,2+}$	24, 70
	$^{6}Li^{2,3+}$	51, 91
	$^{12}C^{3,4,6+}$	71, 101, 174
	$^{16}O^{4+}$	95
B.N.L. (tandem)	$^{6}Li^{3+}$	42
	$^{7}Li^{3+}$	46
	$^{11}B^{2+\text{ to }5+}$	22–50
	$^{12}C^{1+\text{ to }6+}$	19–65
	$^{13}C^{2+\text{ to }6+}$	28–65
	$^{14}N^{2+\text{ to }7+}$	29–79
	$^{16}O^{3+\text{ to }8+}$	28–95
	$^{18}O^{3+\text{ to }8+}$	28–84
	$^{19}F^{2+\text{ to }9+}$	28–93
	$^{32}S^{5+\text{ to }14+}$	50–132
	$^{35}Cl^{14+}$	140
	$^{40}Ca^{14+}$	140
	$^{81}Br^{13+}$	132

2. Experimental procedure

2.1. BEAMS

Light-ion and heavy-ion beams accelerated at the

* Supported, in part, by U.S.E.R.D.A.

† Visiting scientist, Brookhaven National Laboratory, summer, 1975.

University of Michigan cyclotron ($Z=1$–8) and the Brookhaven MP tandem accelerator ($Z=3$–35) were employed. Specific beams and incident energies are listed in table 1. In both accelerators ion species could be rapidly changed, within certain limits, to provide accurate measurements of the Z and A dependence of the scintillator response.

As an example, in the cyclotron beams of the same charge to mass ratio and magnetic regidity are accelerated at nearly the same velocity. Thus by using a suitable gas mixture in the ion source beams of $^4He^{1+}$, $^{12}C^{3+}$ and $^{16}O^{4+}$ could be selected by slight changes in the dee-voltage frequency.

2.2. Spectrometer

Most of the measurements were made with arrangements similar to that shown in fig. 1. The incident beam was collimated to a small spot, typically a few mm in diameter, on a special target foil placed in the center of a scattering chamber. The target consisted of multiple layers of metal foils of different thicknesses so as to degrade the energy of the scattered ion and produce simultaneously a wide range of ion energies. The target and absorber could also be rotated through 90° to provide intermediate foil thicknesses. Ions of a particular momentum-to-charge ratio (p/q) were focused onto one or more scintillator photo-multiplier (PM) detectors located along the focal surface of the spectrometer.

The spectrometer field was deduced from the magnet current or an NMR probe. The resulting error in momentum corresponds to $\lesssim \pm 0.2\%$ uncertainty in the ion energy.

Most of the degraded light ions ($Z<5$) consisted of one charge state ($q=Z$), while the heavier ions often consisted of many different charge states, with $q=Z$ not always having the maximum intensity. In order to facilitate identification, a solid state detector was placed close to the scintillator detectors. This detector, after suitable calibration, provided an energy signal which along with the relative intensities could be used to identify peaks in the scintillator spectrum.

The scintillator response was usually initially measured with elastically scattered ions at a small forward angle ($\theta \approx 10°$) and no absorber, i.e. nearly the full beam energy. The spectrometer field and target/absorber were then changed in small steps so as to follow the scintillator response to lower energies. The lowest energy ions that could be detected were limited by background pulses in the photo-multiplier tubes due to dark noise or γ-rays and neutrons from the beam stop. This limited measurements to $E/A=0.5$–1 MeV/amu.

A few of the ^{12}C and ^{16}O runs with the cyclotron included measurement of the flight time through the spectrometer utilizing the rf pulse structure of the beam and the fast timing signal from the scintillator. This permitted identification and measurements for ions such as ^{13}C and ^{17}O arising from nuclear reactions in the target.

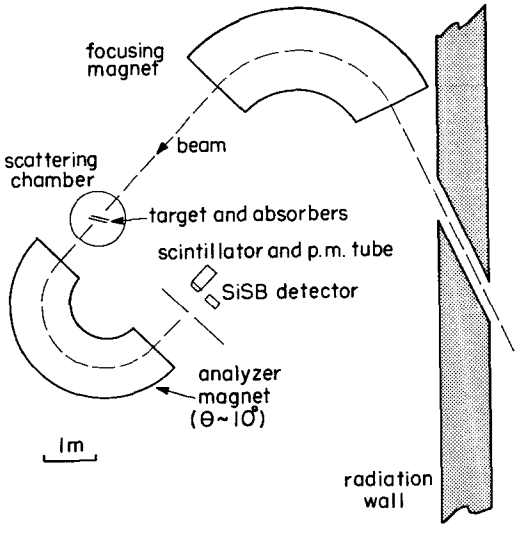

Fig. 1. Typical experimental set-up (UM). A ThC′ α-source (not shown) was located in front of the detectors, in the magnet focal plane.

2.3. Other techniques

Some of the initial measurements were done with techniques different from those described above. In one instance the spectrometer was used but the absorbers were placed directly in front of the detectors. The ion energy was then determined from the solid-state detector. In another set of measurements the PM detector was placed directly in the scattering chamber and the ion energy on the detector varied by changing the direct beam energy and/or the scattering angle. Finally, some ions such as ^1H and ^3He produced in nuclear reactions in the target could be identified and provide additional response data.

2.4. Calibration

An ThC′ α-source ($E=8.78$ MeV) was mounted in the focal-plane to monitor the gain and stability of both the solid-state and scintillator–PM detectors before, after, or during a run. In addition, α-particles and deuterons produced by nuclear reactions in the target often

TABLE 2
Scintillator–PM detector used.

Detector	PM tube[a]	Bias (kV)	Response[b] type	λ_{max}[b] (nm)	Scintillator[c]	λ_{max}[d] (nm)	Light pipe[e]
1	RCA 6342A	+1.3	107(S11)	440	NE102	423	tapered, 5 × 5 cm dia.
2	RCA 6342A	+1.3	107(S11)	440	NE102	423	none
3	RCA 4517	+1.4	115	400	NE102	423	none
4	RCA 8575	−1.4	116	385	NE110	434	none
5	RCA 8575	−1.4	116	385	NE111	375	none

[a] Manufactured by RCA, Inc.
[b] Spectral response and peak wavelength for the tube indicated, as listed in RCA publication PIT-715, *Photo-multiplier selection guide*, RCA Inc. Typical quantum efficiency is 15%.
[c] Nuclear Enterprises, Inc. Front surface aluminized or covered.
[d] Wavelength of maximum scintillator emission, as supplied by manufacturer.
[e] Side surfaces coated with reflective paint and/or aluminum foil. The estimated efficiency is ≈ 80%.

could be identified in the detector spectra and used for calibration purposes. Also, the spectra for heavier ions often consisted of many different charge states and, hence, ion energies. A single spectrum could thus provide many simultaneous measurements of the scintillator response. As an example we display in fig. 2 the spectra obtained in one of the scintillator detectors for various charge groups of ^{35}Cl ions observed at one particular magnetic field setting.

A serious problem was observed using detectors with high gain "fast" PM tubes, however. This will be discussed separately below.

2.5. SCINTILLATOR–PM DETECTORS

The scintillator–PM combinations employed are listed in table 2. The scintillator was typically 6 mm thick. The scintillator front surface was either aluminized (≈100 μg/cm²) or covered with a thin (≈1 mg/cm²) aluminum reflector foil. The scintillator was directly coupled to the PM tube with optical grease or through a short (1″) tapered light-pipe attached to the PM tube. A thick (≥6 mm) cylindrical aluminum cap with a 6 mm hole located near the center served to locate the scintillator and act as a collimator restricting the area of the scintillator exposed to the incident ions. The PM tubes were enclosed in magnetic shields to minimize the effect of the spectrometer fringing fields. Their effectiveness was verified by direct field measurements with a gaussmeter and measurement of PM tube response as a function of the spectrometer field with an α-source.

The PM tubes were mounted in tube bases similar to the Ortec model 265 and 266 bases[13]). The high-voltage was applied to the anode of the 6342A and 4517 tubes and the cathode of the 8575 tubes[14]). The output signal was taken from the anode across a load resistor via a large, hv blocking capacitor. The anode pulses were sent directly or via a fast pre-amp to a delay-line amplifier[13]) (Ortec-460) with an integration time constant ≈40 ns. Tests were made to determine the effects of different pre-amps, post-amps, time constants, etc. No large differences (i.e. > 10%) in the relative outputs were observed that could be ascribed to the electronics. The signals were digitized and stored in an on-line computer or multichannel analyzer.

As can be seen from table 2, two basic types of PM tubes were utilized: mono-alkali photo-cathode type

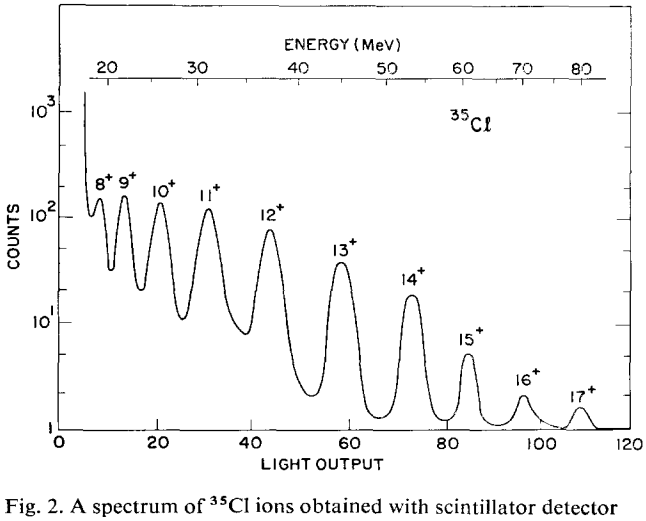

Fig. 2. A spectrum of ^{35}Cl ions obtained with scintillator detector no. 4. The ion charge state and energy are indicated.

having a circular cage dynode structure (RCA 6342A), and a newer design, high-gain bi-alkali photo-cathode type having an in-line dynode structure (RCA 8575). While the latter type tubes exhibited superior performance in terms of dark current noise and hence pulse height resolution (by factors of about ten and two, respectively) they also could be non-linear (ca. 20%) at least with the tube bases used, exhibiting tube saturation effects when operated at the recommended voltages (−1800 V).

These effects were noted by observing the ratio of anode pulse heights for different ions in the scintillators as a function of PM high voltage. The typical non-linearity tended to make the scintillator light output appear to be more linear with ion energy than it actually was. It was therefore decided to run the 8575 tubes at a lower voltage (−1400 V) and remove any non-linearities by calibrating the detectors using a light pulser. In this way it was possible to distinguish the PM tube non-linearity from that of the scintillator itself. Fortunately, most of the data were obtained using low-gain tubes which did not require corrections for non-linearity.

In retrospect, it appears that the use of fast, high-gain multi-alkali tubes such as the RCA 8575 for scintillation pulse-height measurements requires special precautions[15]). In particular a voltage-divider network designed to minimize space-charge effects at the last dynode should be used[15]). Timing measurements utilizing the pulsed cyclotron beam, however, indicate that most PM tubes (table 2) are capable of moderately fast timing (≤ 2 ns) adequate for many applications. A low-gain, low-noise PM tube may therefore be preferable to fast, high-gain timing PM tubes in certain applications, particularly if the light collection efficiency is increased, e.g. by using a larger diameter tube.

3. Experimental results

3.1. Uncorrected light output

The light output, L, as deduced from the measured anode signal of detector 1 (table 2) is shown in fig.4 as a function of ion type and energy. The ion energies have been corrected for energy losses[16]) in the front-surface reflector *but* not for apparent losses in the scintillator itself (i.e. due to "dead" layers). Also the non-linearity of the PM tube has not been removed although this is negligible for the particular PM used (6342A). The units for L have been arbitrarily chosen for convenience and correspond to $L=30$ for ThC′ α-particles ($E=$ 8.78 MeV). No attempts were made to measure the absolute light output. This paper will always refer to relative light output, unless otherwise noted.

The data shown in fig. 3 represent several sets of measurements taken with the seme detector at two different laboratories (UM and BNL). The agreement between different sets of data obtained with the same detector is very good (within a few percent). Consistent differences, however, were observed for some of the data for the same ions obtained with different detectors, even when known PM tube non-linearities were removed. These differences were most apparent in the low energy portions of the response curves and for the heavier ions ($Z \geq 8$). The data for detector 1, e.g., indicated a much faster decrease in L with decreasing energy than those for the other detectors. Also, the light output for $Z>8$ was substantially less for detector 1. This is shown in fig. 4 where we compare the output of detectors 1 and 4 (table 2). The differences in light output for these detectors are consistent with the presence of a thin non-light-producing "dead" layer (2–10 μm) on the front surface of the scintillator of detector 1. Although the exact origin of such layers is uncertain, it is known that oxidation can degrade the

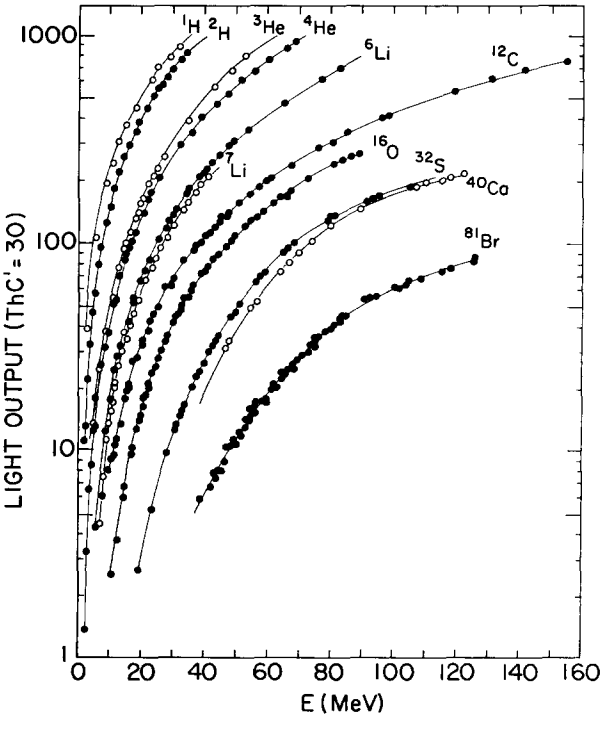

Fig. 3. Response of scintillator detector no. 1 in units such that ThC′ α-particles (8.78 MeV) have an output of 30. The energies have been adjusted for losses in the front-surface reflector material but not for any additional effects (see text).

light output of plastic scintillators[18]), Since the scintillator material used in detector 1 was several years old and had not been initially aluminized whereas the other scintillators had been. it is perhaps not surprising that it exhibited a noticeable "dead" layer. Aluminizing or similar protection of scintillator front surfaces therefore appears to be advisable particularly in heavy-ion applications.

3.2. Differences in scintillator response

As seen in table 2, several different types of scintillators were utilized. Although differences in the relative response were observed for ions with $Z \gtrsim 8$ (fig. 4), we do not ascribe these differences to the scintillator composition as they were associated more with the particular piece of scintillator used rather than its composition. Different types of scintillators prepared under similar conditions produced relative light outputs equal to within 10% for ions $Z=1$ to $Z=16$. We therefore conclude that the intrinsic light output for the scintillators used (table 2) is essentially the same but that other effects, as noted in the previous section, may cause differences in the heavy-ion response of scintillator detector systems.

3.3. Scintillator response, $L(E, Z, A)$

We have combined data from several detectors to infer the "typical" response of plastic scintillators to heavy ions. Most of the data incorporated was that for NE102, although some of the data for NE110 and NE111 was utilized to obtain the relative response for different isotopes (e.g. ^{16}O vs ^{18}O). The scintillator light output has been deduced from the raw detector response curves, such as fig. 3, by removing the non-linearity of the PM tubes and the effect of any *apparent* front surface "dead" layer. The latter is a relatively small correction (a few percent) except for $E/A \leq 2$ MeV/amu and/or $Z \geq 20$, where the corrections may be as large as 50%. The final results are shown in fig. 5. Data which include significant corrections are denoted by dashed lines. All the data except the latter have an estimated uncertainty of $\pm 5\%$ or less. The other data are less accurate than this, but are likely good to $\pm 20\%$ or better.

The curves displayed in fig. 5 represent the response expected for typical plastic scintillators, front-surface aluminized, with ions at near-normal incidence. The "intrinsic" scintillator response is likely to be larger, particularly for $Z>20$ and/or $E/A<2$ MeV/amu for the following reasons: Firstly, energetic secondary electrons are thought to play a dominant role in determining the response for the heavier ions (see sect. 5). If so, the scintillator response will depend on the mode of incidence of the particular ion and the geometry of the scintillator, e.g. the number of surfaces traversed by the ion. Secondly, there may always be a certain

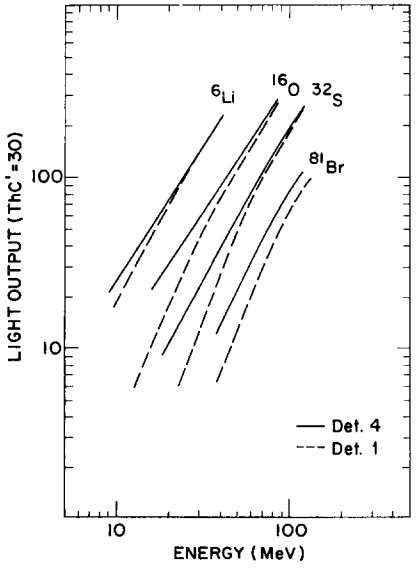

Fig. 4. Comparison of the response of scintillator detectors 1 and 4 (table 2).

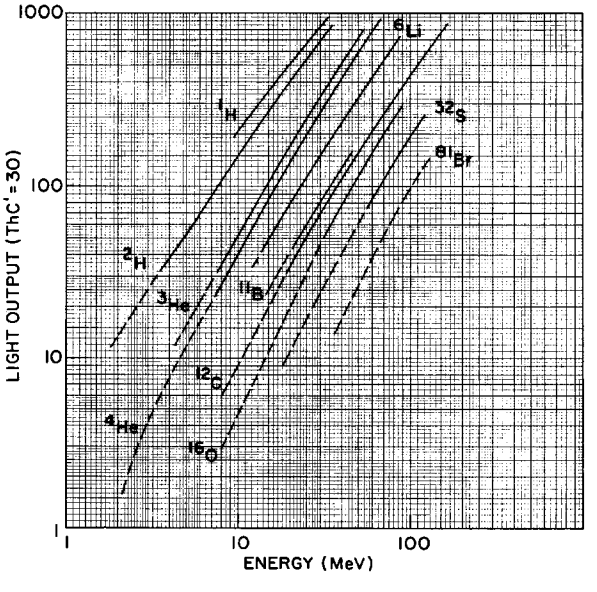

Fig. 5. Inferred scintillator output for typical plastic scintillators such as NE102 for near-normal incident heavy ions. Estimated uncertainty is ± 5% except for dashed curves which are likely lower limits to the intrinsic response and have ± 20% or greater uncertainty (see text).

thickness of inactive material on the scintillator surfaces. Both of the effects noted above will result in a lower response for a front surface detector or TFD relative to the intrinsic response. There is some evidence for this: The relative response of fission fragments ($Z \approx 90$, $E \approx 100$ MeV), detected from sources imbedded in organic scintillators is about a factor of two larger than that deduced using the ^{81}Br curve shown in fig. 5. The effects noted above while pertinent for $Z \geq 20$ and/or $E/A \lesssim 2$ MeV/amu (dashed curves fig. 5) will affect only slightly (<10%) the results obtained for other ions and energies. The actual response observed with a particular scintillator must, of course, include consideration of energy losses in the front surface reflector, if any, losses in "dead" layers, if known, and the non-linearity of the PM detector. The former effects will normally reduce the light output for all the low energy ions as well as the more massive ions (fig. 5) whereas the typical PM non-linearities, tube saturation or space-charge effects, will "flatten" the response curve as a function of increasing light output, and hence ion energy[15]).

The response curves, figs. 3 and 5, qualitatively resemble those obtained for NaI ($5 \leq Z \leq 10$) where the data overlap[2,3]) and those for glass dosimeters[19]) ($1 \leq Z \leq 6$). The agreement with other data available for heavy ions stopped in plastic scintillators is fair[20–22]). The previously published data, however, are not extensive and include mostly measurements at relatively high energies ($E/A > 6$ MeV/amu). The data available [4,5]) for TFD are not directly comparable to those for stopped ions as the former are mostly for transiting ions.

We note several features in the observed response data (for clarity, not all of the data are included in the figures):

a) The light output, L, is non-linear with ion energy at low energies, becoming more linear for $E/A \gg 6$ MeV/amu.

b) The non-linearity of L with energy is similar for all ions within the same velocity range, i.e. $L \propto E^n$ with $n \approx$ constant independent of Z and A ($n \approx 1.6$).

c) The light output is slightly less (ca. 5%) for odd-Z ions compared to that for adjacent even-Z ions ($Z \approx \frac{1}{2}A$).

Features similar to (a) and (c) have been observed previously for inorganic scintillators[2,3]). Organic plastic scintillators have been suggested to be linear with energy, even for heavy ions[20]), although this may be true at higher energies[21,22]).

3.4. Resolution

Along with the relative light output L we have measured δL, the fwhm resolution in L. Note that since $L \propto E^n$, where $n \geq 1$, then $\delta E/E \leq \delta L/L$. At low values of L ($L < 100$ units), δL was limited by the PM tube noise or the background counting rate, while at high energies δL was limited by the photon counting statistics ($\delta L \propto \sqrt{L}$). No special attempts were made to optimize δL, although the scintillators were well collimated.

We find specifically that

$$\delta L^2 \approx \delta L_S^2 + \delta L_T^2, \tag{1}$$

where δL_S is the intrinsic resolution of the scintillator and detector geometry while δL_T is the degradation due to the electronics and PM tube noise. In the units of fig. 5, $\delta L_T \approx 5$ for detectors 1 and 2 and $\delta L_T \approx 0.6$ for the other detectors. We then find emperically that

$$\delta L_S = 0.8 \sqrt{L}, \tag{2}$$

with perhaps a slight dependence on Z, resulting in better resolution for heavier ions compared with less energetic light ions producing the same light output. Certainly, unlike solid-state detectors, δL_S is not proportional to $\sqrt{E}$ even for light ions.

Eq. (2) implies that the number of photoelectrons detected is approximately equal to L, our units for light output. The actual number of photons produced in the scintillator is ten to twenty times greater owing to the PM tube and light collection efficiencies[18]). Fig. 5 is essentially a plot of the number of photoelectrons produced at the PM photo-cathode vs ion energy and species. At $E/A = 5$ MeV/amu, for example, the average energy required per photoelectron for ^{1}H, ^{4}He, ^{12}C, ^{32}S and ^{81}Br ions is 50, 130, 300, 420 and 450 keV, respectively. The required energy per scintillator photon is then about 5, 13, 30, 42 and 45 keV, respectively, due to the aforementioned estimated light-conversion efficiency. These values depend strongly on the ion energy, however, indicating a complicated mechanism for the photon production in the scintillator.

Our results indicate that for $L > 500$, $\delta L/L \lesssim 3\%$ fwhm, relatively independent of the ion species, In contrast, the resolution of a solid-state detector degrades rapidly with increasing ion mass due to nuclear stopping[25]). In fact, it appears that the intrinsic scintillator energy resolution, $\delta E/E (\leq \delta L/L)$ for very heavy ions ($Z > 35$) may approach that possible with existing solid-state detectors. Furthermore, the resolution of plastic scintillators is comparable[2]) to that of

TABLE 3

Parameterizations of light output.

Parameter set	Data[a]	Energy range (MeV/amu)	Parameterization	χ^2/N [b]	Comment
I	plastic (includes all isotopes)	$0.5 \leq E/A \leq 15$	$L = (4.0)(ZA)^{-0.63}E^{1.62}$	12.0	More correct A dependence
II	plastic (only data of fig. 5)	$0.5 \leq E/A \leq 15$	$L = (4.57)Z^{-0.26}A^{-0.93}E^{1.62}$	9.5	Valid $A \approx 2Z$ only
III	plastic (fig. 5, excluding $Z = 1$)	$0.5 \leq E/A \leq 15$	$L = (3.66)Z^{-0.08}A^{-1.0}E^{1.63}$	4.6	Valid $A \approx 2Z$ only
IV	plastic (fig. 5)	$0.5 \leq E/A \leq 15$	$L = (1.58)Z^{+1.22}(R - 0.042Z)$ [c]	7.6	Best over-all description

[a] This work. The data included in the fitting procedure are indicated.
[b] Chi-square per data point (see text).
[c] R is the ion range in mg/cm^2 where $R(\text{NE102}) = 1.13\,R(\text{CH}_2)$, and $R(\text{CH}_2)$ is the semiemperical value tabulated in ref. 16.

NaI(Tl) for energetic ions. The relatively poor resolution, δL, quoted for some plastic-scintillator detector systems is therefore likely due to poor light-collection efficiency or low scintillator light output. It appears that in many applications scintillators are competitive with other types of detectors for massive, energetic heavy ions.

4. Analysis

4.1. Parameterization of $L(E, Z, A)$

We have fit the response curves (fig. 5) with simple parameterized expressions for L as a function of E, Z, and A. Generalized non-linear least-squares fitting techniques were employed[23]). Instead of minimizing the total χ^2 summed over all data points, however, we have minimized instead the χ^2 per data point per data set, summed over all data sets, where a data set consists of the response data for a specific ion. Thus each ion, is given equal weighting. Certain constraints were also placed on the range of ion velocities (E/A) used in the fitting procedure. This was done primarily to allow exclusion of the high energy light-ion data which exhibits characteristics different from the other data.

The results of some of the more successful parameterizations are listed in table 3 together with the resulting χ^2 per point, χ^2/N, where $\chi^2/N \leq 1$ indicates a perfect fit. We observe that $L \propto E^n$, where $n \approx 1.6$, $E/A < 15$ MeV/amu. The precise dependence on Z and A is more difficult to determine since $Z = \frac{1}{2}A$ for most of the heavy ion data. An analysis of the available data for different isotopes of the same element (^{1,2}H, ^{6,7}Li, ^{12,13}C, ^{16,17,18}O) indicates that $L \propto A^{-m}$ with $m \approx 0.6$ (Z,E constant) whereas for different elements $L \propto Z^{-p}$ with $p \approx 0.1$ (E constant, $A \approx 2Z$).

Although the parameterizations of L are useful for interpolations and possibly extrapolations of the empirical data (fig. 5) they do not reproduce the original data to better than about $\pm 20\%$ on the average. It is more accurate to interpolate or extrapolate directly from the response curves displayed in fig. 5.

4.2. Response vs ion range

In the limit of complete saturation of the scintillator light output ($dL/dx \approx$ constant, see sect. 3), one would expect L to be proportional to the ion range, R, in the scintillator. This has been found to be the case for low-energy α-particles[24].) Such a picture would account for the observed energy dependence of L (table 3) since $R \propto E^n$ with $n \approx 1.7$ for low-energy heavy ions[25]).

We display in fig. 6 the relationship between L and

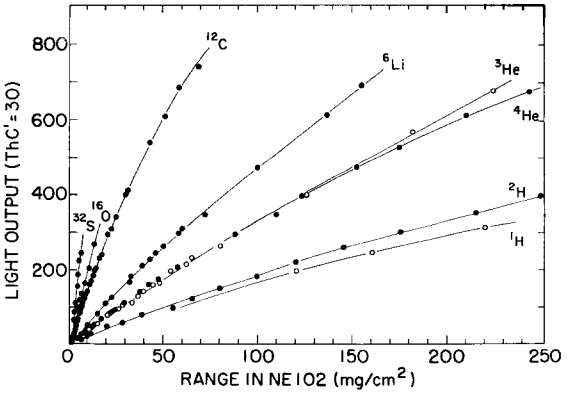

Fig. 6. Scintillator response vs the calculated ion range. The latter have been obtained assuming $R(\text{NE102}) = 1.13\,R(\text{CH}_2)$ with $R(\text{CH}_2)$ taken from ref. 16.

R for different ions as deduced from the data of fig. 5. The ion ranges have been calculated using the range tables of Northcliffe and Schilling[16]) assuming $R(\mathrm{NE102}) = 1.13\,R(\mathrm{CH_2})$. As can be seen in fig. 6, L is approximately proportional to the ion range[12]) with a strong dependence on Z but little if any dependence on the isotope mass, A. The L vs R data exhibit a noticeable curvature and a non-zero intercept, particularly for the heavier ions ($Z>8$). These effects are not likely due to "dead" layers as the effect of these have been removed (sect. 3.1). Rather, it appears that the effective, light-producing portion of the range, R_L, is less than the total ion range. The difference $\Delta \equiv R - R_L$ is about 2 μm ($Z=6$), 5 μm ($Z=8$), 10 μm ($Z=16$) and 15 μm ($Z=35$) in the scintillator ($\rho = 1.03$ g/cm^3). There may be several effects which contribute to Δ: (a) Light-producing secondary electrons (see sect. 5) may be ejected from the front surface reducing L. This effect would be most important for ions having a short range. (b) Near the end of the ion's range neutralization via electron capture becomes important. The primary ionization, hence L, will be reduced and the ion's range extended. Effects similar to (a) and (b) have been observed for ion tracks in photographic emulsions[26]). Both effects should become more important with increasing Z. In photographic emulsions ($\rho = 3.5$ g/cm^2) for example, the effect of (b) is to extend the ion range by typically 8 μm ($Z=6$), 12 μm ($Z=8$), 18 μm ($Z=10$) and 32 μm ($Z=20$).

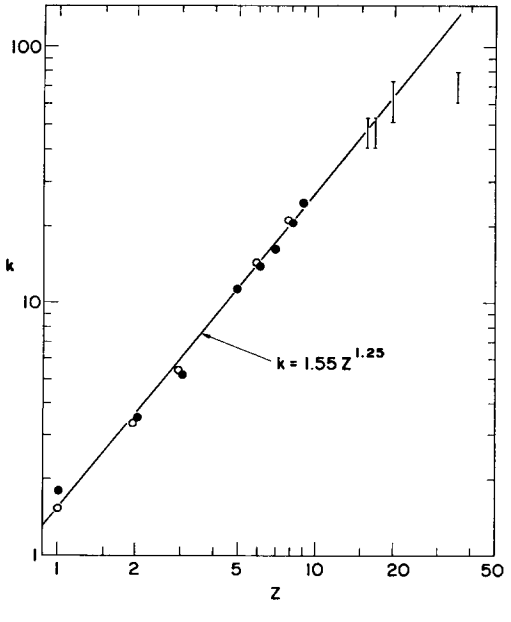

Fig. 7. The function $k(Z)$ vs Z [eq. (3)]. The error bars correspond to the limits $\Delta(Z) = 0$ and $0.04\,Z$ mg/cm^2, respectively.

This is qualitatively similar to the phenomena observed here.

The empirical relation between L and R is given approximately by

$$L = k(Z)\,R[1 - \Delta(Z)], \tag{3}$$

where R is the calculated ion range (mg/cm^2), $k(Z)$ is a Z-dependent coefficient and $\Delta(Z)$ represents the non-light-producing fraction of R. The quantity $\Delta(Z)$ depends principally on Z and is relatively independent of E. Application of eq. (3) to the scintillator data of fig. 5, $0.5\ \mathrm{MeV/amu} \leq E/A \leq 15\ \mathrm{MeV/amu}$ yields the values of $k(Z)$ and $\Delta(Z)$ given in table 3. The parameterization (3) is substantially better than others and is therefore the preferred one for interpolation purposes. The coefficients $k(Z)$ and $\Delta(Z)$ both increase with increasing Z as is shown in fig. 7 where we display $k(Z)$ vs Z for our data. Note that R is the calculated range so that variations in $k(Z)$ and $\Delta(Z)$ may be due in part to deviations of the true ion range from the calculated ones. More extensive experimental range–energy data for even-Z and odd-Z ions in organic materials would be very useful.

A remarkable feature of eq. (3) is that, except for a renormalization constant, one can adequately describe with nearly the *same* coefficients $k(Z)$ and $\Delta(Z)$ the data available for the light output of NaI for heavy ions[3]). Thus for heavy ions L depends primarily on the incident ion species (Z,A) and range and not the luminescent properties of the particular scintillator. This evidence strongly favors the delta-ray description of the light-producing process[7–10]) (see sect. 5).

4.3. Scintillation efficiency, dL/dE

Differentiation of $L(E)$ with respect to ion energy gives the relative scintillator efficiency, dL/dE. We have deduced dL/dE from the plastic-scintillator data by numerical differentiation of the smooth empirical curves shown in fig. 5. We display dL/dE vs E/A and vs dE/dx in figs. 8 and 9. Energy losses have been calculated from the tables of Northcliffe and Schilling[16]), assuming $dE/dx(\mathrm{NE102}) = 0.88\ dE/dx(\mathrm{CH_2})$. The coefficient 0.88 is a correction based on the different carbon/hydrogen ratios in NE102 and CH2 (1:1.104 and 1:2, respectively).

It can be seen in fig. 8 that dL/dE in general is not constant, except at high energies ($E>40$ MeV). The variation of dL/dE with energy is somewhat similar for different ions, but the magnitude depends on Z, descreasing with increasing Z.

The data of dL/dE vs dE/dx (fig. 9) exhibit the well-

known[27]) saturation effect of solid scintillators, i.e. dL/dE decreases rapidly with increasing dE/dx. However for ions having the same specific energy loss the efficiency dL/dE increases with increasing Z. The present data obtained for plastic scintillators are qualitatively similar to those reported for NaI [3]) although, of course, dE/dx is different for the two media.

We present an interpretation of these results in sect. 5.

4.4. Specific fluorescence, dL/dx

The specific fluorescence, which is the scintillation output per path length, dL/dx, can be deduced from the scintillation efficiency, dL/dE, and the specific energy loss, dE/dx, since $dL/dx=(dL/dE)\times(dE/dx)$. The quantity dL/dx is of particular importance as it is related to the radiation damage and dose rate of ions in solids[8,9]). Also, dL/dx is expected to exhibit a simple functional dependence on dE/dx, and thus it is the focus of many of the models constructed to describe scintillation processes[4–10]).

Using available values[16,17]) of dE/dx and the semi-empirical dL/dE data (figs. 8 and 9) we obtain the dL/dx values shown in fig. 10. Again, the results are qualitatively similar to those obtained for NaI [3]) and, also, plastic TFD where data overlap[4,5]). We also include in fig. 10 data published for minimum ionizing particles[21]) and an extrapolation to large values of dE/dx.

The following features are observed:

a) The quantity dL/dx is not a simple function of dE/dx, at least for the data shown in fig. 10.

b) At the same value of dE/dx, dL/dx increases with increasing Z, but is relatively independent of mass (A),

c) dL/dx can be double valued with respect to dE/dx for large dE/dx.

Some of these features have been noted previously for NaI [3]) and plastic TFD scintillators[4,5]). The data for the TFD should be directly comparable to ours. Although the behaviour of dL/dx vs dE/dx is similar, the relative values are somewhat different, being slightly lower for heavier ions in the TFD relative to our data. These differences are likely due to the particular construction of the TFD and the method of light collection used for this detector. Surface effects, for example may be more important for the TFD, which would reduce the light output for the heavier ions (see sect. 3).

In general, the results shown in fig. 10 indicate that neither $dL/dx \propto dE/dx$ (no saturation) nor $dL/dx=$ constant (complete saturation) is a good approximation although for moderately energetic "light" heavy ions ($2<Z<8$) the latter is more accurate. Minimum ionizing particles such as cosmic rays however, exhibit a quite different behavior, with dL/dx proportional to dE/dx, even for heavy ions[21]).

5. Scintillation theory

We present here an interpretation of the scintillator response data based on the Murray–Meyer (MM) model[7]) as many of the effects observed can be understood with this simple model.

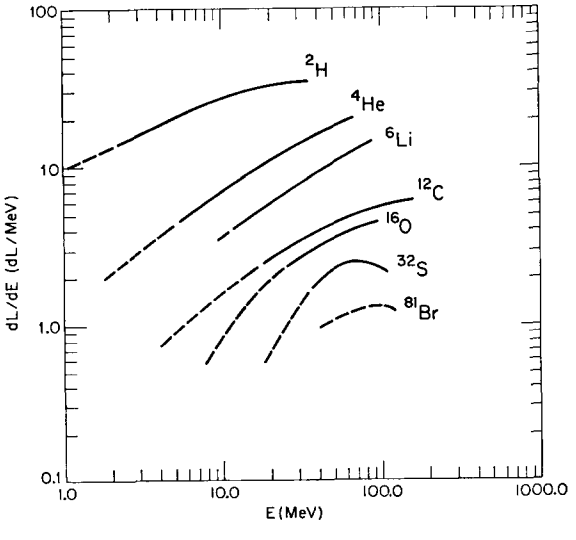

Fig. 8. Scintillation efficiency vs energy [$L(\mathrm{ThC}'\,\alpha)=30$]. The solid and dashed curves correspond to the data shown in fig. 5, with errors ± 5% and ca. ± 20% or greater, respectively.

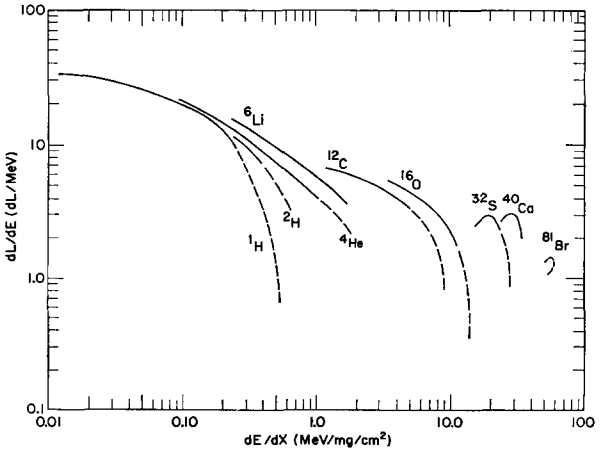

Fig. 9. Scintillation efficiency vs the calculated specific energy loss in NE102. The latter are from ref. 16 assuming $dE/dX(\mathrm{NE102}) = 0.88\,dE/dx(\mathrm{CH_2})$. Otherwise same as fig. 8.

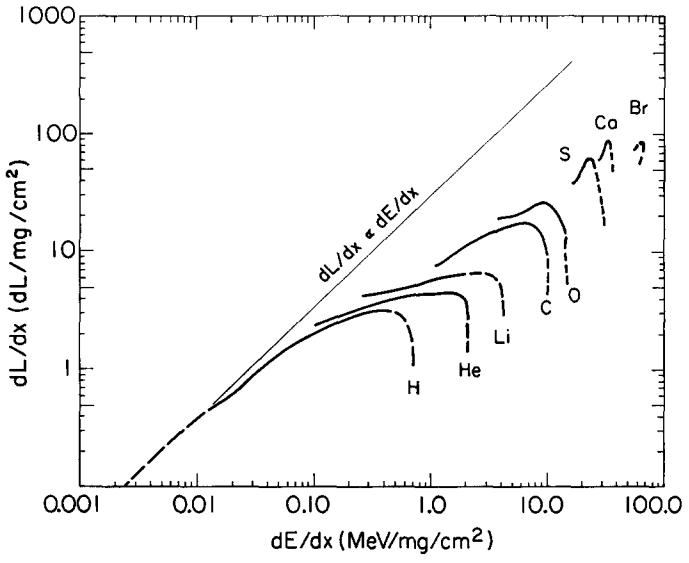

Fig. 10. Specific fluorescence vs calculated specific energy loss in NE102. Otherwise same as fig. 8.

The MM model proposes that the specific fluorescence, dL/dx and scintillation efficiency, dL/dE, arise from two sources: (1) a primary column of ionization centered along the path of the incident ion and (2) energetic secondary electrons (δ-rays) which escape beyond the primary column. Along the primary column, dL/dE is a function of dE/dx and for large dE/dx, dL/dE exhibits saturation[27]). The characteristics of dL/dE along the primary column depend on the composition of the scintillator, including the activator concentration[27]). Also, the radius of the primary column, which is few hundred Ångstroms, may have a weak dependence on dE/dx or the incident ion type[7,26]) The energetic δ-rays (1–20 keV) however, produce light with high efficiency ($dL/dE \approx 1$) compared to the scintillation efficiency of the primary column ($dL/dE \ll 1$) [27]). The density of δ-rays depends on Z and E/A of the incident ion as well as dE/dx [7,9,26]). (Note: The units for dL/dE used in this section are different from those used in sect. 4 and figs. 8–9).

Thus, MM propose that

$$\frac{dL}{dx} = \left(\frac{dL}{dx}\right)_p + \left(\frac{dL}{dx}\right)_\delta$$

$$= \left(\frac{dL}{dE}\right)_p \left(\frac{dE}{dx}\right)_p + \left(\frac{dL}{dE}\right)_\delta \left(\frac{dE}{dx}\right)_\delta, \tag{4}$$

or upon dividing by $dE/dx = (dE/dx)_p + (dE/dx)_\delta$

$$\frac{dL}{dE} = (1-F)\left(\frac{dL}{dE}\right)_p + F\left(\frac{dL}{dE}\right)_\delta, \tag{5}$$

where

$$F = \frac{(dE/dx)_\delta}{dE/dx} \tag{6}$$

The subscripts p and δ refer to the primary column and δ-rays, respectively. The quantity F, which is a function of Z and E/A, represents the fraction of energy loss of the incident ion which is deposited outside of the primary column, i.e., in the δ-rays[7]). Minimum ionizing, low-Z particles have $(dE/dx)_p \gg (dE/dx)_\delta$ and therefore dL/dx and dL/dE are determined mainly by $(dL/dE)_p$. The scintillator models of Birks[28]) and Wright[29]), are primarily concerned with determining $(dL/dE)_p$ and $(dL/dx)_p$ as these can be expressed as simple functions of dE/dx. Heavy ions have $(dL/dE)_p \ll 1$, due to saturation, therefore eq. (5) can be simplified since for energetic electrons $(dL/dE)\delta \approx 1$ (in appropriate units), thus

$$\frac{dL}{dE} \doteq (1-F)\left(\frac{dL}{dE}\right)_p + F, \tag{7}$$

and therefore

$$\frac{dL}{dX} = \left[(1-F)\left(\frac{dL}{dE}\right)_p + F\right]\frac{dE}{dx} \tag{8}$$

The fluorescence dL/dE and dL/dx for heavy ions is then determined by $F(Z, E/A)$ as well as $(dL/dE)_p$, i.e., the δ-ray production and the saturation of the primary column.

The qualitative features predicted by the MM model are in accord with the data for both NaI(Tl) and plastic scintillators. At low dE/dx ($\lesssim 0.1$ MeV.mg^{-1} cm^2), dL/dE and dL/dx are determined by the behavior of $(dL/dE)_p$, i.e., the first terms of eqs. (4) and (5). Thus dL/dx and dL/dE (figs. 9 and 10) are then mainly functions only of dE/dx [$\approx (dE/dx)_p$] since [7]) $F \approx 0.2$. It has been shown previously that for minimum ionizing particles $dL/dx \propto (dE/dx) \times [1 + kB(dE/dx)]^{-1}$ where kB is about 10 mg/cm^2 MeV for NE102 plastic[21]) and about 7 mg/cm^2 MeV for CSI, NaI and anthracene[29]).

The fluorescent response for heavy ions, however, is more complicated as $(dL/dE)_p$ is small (<0.5) while $F \approx 0.2$. The second terms in eqs. (4) and (5) are then important. One therefore observes a marked dependence of dL/dE and dL/dx on the Z and E/A of the incident ion since the δ-ray production depends on these quantities (figs. 9 and 10). In the limit $(dL/dE)_p \to 0$, $dL/dx \to F(Z, E/A) dE/dx$ and $dL/dE \to F(Z, E/A)$. Thus while, energetic light ions may exhibit L linear with E, i.e. $dL/dE \doteq$ constant, heavy ions in general do not, although at high energies the function $F(Z, E/A)$ becomes a slowly varying function of E/A. At lower energies $F(Z, E/A)$ decreases[7]) with decreasing E/A, i.e., the δ-ray production is proportional to the incident ion velocity. Also, since $F(Z, E/A)$ is an atomic property it can be expected to be similar for plastic, NaI, etc. These features are, in fact, consistent with our observations (sect. 4).

MM applied their model to the data then available for NaI(Tl). They deduced an empirical $F(Z, E/A)$ and compared it to predicted functions[7]). Qualitative agreement was obtained, indicating that $F(Z, E/A)$ was relatively independent of Z, but, as expected, $F(Z, E/A)$ increased with E/A with $F \lesssim 0.25$ up to $E/A = 10$ MeV/Amu. At the time of their analysis, however, dE/dx for heavy ions in NaI was poorly known and therefore calculated values were used. This introduces considerable uncertainties in their results.

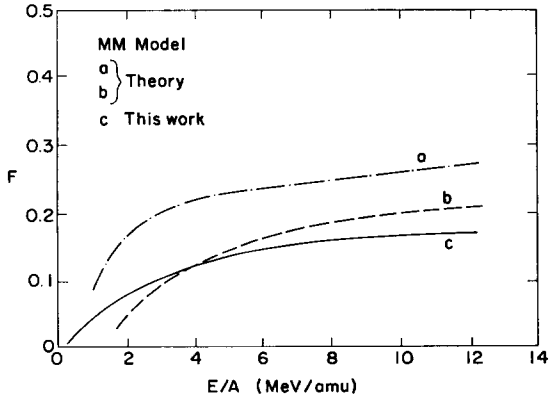

Fig. 11. A comparison of the function F [eqs. (7) and (8)], as deduced from our dL/dE and dL/dx data, with calculations from ref. 7.

We have applied the MM model to our data for plastic scintillators. The function $(dL/dx)_p$ was taken to be that measured for the organic crystal anthracene[27]), which is similar in physical composition and fluorescence to plastic scintillator[27]). The function $F(Z, E/A)$ was then deduced from the dL/dE data using eq. (8). Our results are shown in fig. 11. The function $F(Z, E/A)$ deduced for plastic scintillator closely resembles the functional form predicted by MM. A reanalysis of the NaI data[3]) using realistic[16]) values for dE/dx, yields a function $F(Z, E/A)$ resembling our curve and the MM predictions.

As can be seen in fig. 11, F varies from 0.1 to 0.2 for $E/A > 2$ MeV/amu, i.e., 10–20% of the incident ion energy loss is deposited as δ-rays. In the same energy range $(dL/dE)_p < 0.5$ for $Z \geq 2$ so δ-ray production becomes increasingly important for ions heavier than ^{4}He. As an example our results indicate that δ-ray production accounts for about 8%, 20%, 40%, and 75% of the specific fluorescence of ^{1}H, ^{4}He, ^{6}Li and ^{16}O at $E/A \approx 5$ MeV/amu. Although more refined scintillator models are available and probably more realistic[8–10]) many of the basic features of scintillator response can be explained in terms of the simple MM model, at least phenomenologically.

One of us (F.D.B.) thanks the staff at Brookhaven laboratory for their hospitality and financial support while a summer visitor at BNL. Useful discussions with B. G. Harvey and R. Katz are also gratefully acknowledged.

References

1) G. L. Miller et al., Nucl. Instr. and Meth. **91** (1971) 389; B. G. Harvey et al., Nucl. Instr. and Meth. **104** (1972) 21; E. Beardsworth et al., Nucl. Instr. and Meth. **127** (1975) 29.

2) A. R. Quinton, C. E. Anderson and W. J. Knox, Phys. Rev. **115** (1959) 886.

3) E. Newman and F. E. Steigert, Phys. Rev. **118** (1960) 1575.

4) L. Muga and G. Griffith, Nucl. Instr. and Meth. **109** (1973) 289; ibid. **111** (1973) 581; R. K. Batra and A. C. Shotter, ibid. **124** (1975) 101; T. Batsch and M. Moszynski, ibid. **125** (1975) 231; Luis Muga, ibid. **125** (1975) 541.

5) L. Muga and G. Griffith, Phys. Rev. **B9** (1974) 3639.

6) Nuclear Enterprises, Inc. San Carlos, Calif., U.S.A.

7) R. B. Murray and A. Meyer, Phys. Rev. **122** (1961) 815; A. Meyer and R. B. Murray Phys. Rev. **128** (1962) 98.

8) R. Katz and E. J. Kobetich, Phys. Rev. **170** (1968) 397; ibid. p. 401; E. J. Kobetich and R. Katz, op. cit. p. 391 and p. 405.

9) R. Katz, S. C. Sharma and M. Homayoonfar, Nucl. Instr.

and Meth. **100** (1972) 13; R. Katz and F. E. Pinkerton, ibid. **130** (1975) 105.
[10]) L. Muga and M. Diksic, Nucl. Instr. and Meth. **122** (1974) 553.
[11]) P. B. Price, E. K. Shirk, W. Z. Osborne and L. S. Pinsky, Phys. Rev. Lett. **35** (1975) 487.
[12]) F. D. Becchetti, Bull. Am. Phys. Soc. **20** (1975) 602; F. D. Becchetti, C. E. Thorn and M. J. LeVine, Bull. Am. Phys. Soc. **21** (1976) 109.
[13]) Ortec, Inc. Oak Ridge, Tenn. U.S.A.
[14]) RCA Inc., Harrison, N.J., U.S.A.
[15]) RCA Photomultiplier Manual (RCA Inc., Harrison, N.J., 1970) pp. 30, 103; H. J. Lush, J. Sci. Instr. **42** (1965) 597; P. L. Land, Rev. Sci. Instr. **42** (1971) 420.
[16]) L. C. Northcliffe and R. F. Schilling, Nucl. Data **A7** (1970) 233.
[17]) J. Tripier et al., Nucl. Instr. and Meth. **115** (1974) 29.
[18]) J. B. Birks, *The theory and practice of scintillation counting* (Pergamon Press, Oxford, 1964).
[19]) R. H. Schuler, J. Phys. Chem. **71** (1967) 3712; R. H. Schuler and A. O. Allen, J. Am. Chem. Soc. **63** (1959) 808.
[20]) E. Newman, A. M. Smith and F. E. Steigert, Phys. Rev. **122** (1961) 1520.
[21]) G. D. Badhwar, C. L. Deney, B. R. Dennis and M. F. Kaplon, Nucl. Instr. and Meth. **57** (1967) 116.
[22]) B. G. Harvey, F. Pühlhofer and J. Mahoney, private communication; M. Buenerd et al., Nucl. Instr. and Meth. **136** (1976) 173.
[23]) Subroutines ZPOWL and PRAXIS (unpublished).
[24]) J. R. Prescott and A. S. Rupoal, Can. J. Phys. **39** (1961) 221.
[25]) R. D. Evans, *The atomic nucleus* (McGraw-Hill, New York, 1955) p. 652.
[26]) H. H. Heckman et al., Phys. Rev. **117** (1960) 544.
[27]) J. B. Birks, op. cit., ch. 11, sect. 3.
[28]) J. B. Birks, Proc. Phys. Soc. **A64** (1951) 874.
[29]) G. T. Wright, Phys. Rev. **91** (1953) 1282.